Spin-resolved commensurability oscillations

J. P. Lu and M. Shayegan
Department of Electrical Engineering, Princeton University, Princeton, New Jersey 08544

L. Wissinger and U. Rössler
Institut für Theoretische Physik, Universität Regensburg, D-93040 Regensburg, Germany

R. Winkler
Institut für Technische Physik III, Universität Erlangen Nürnberg, D-91058 Erlangen, Germany
(Received 24 September 1998; revised manuscript received 4 February 1999)

We report the observation of commensurability oscillations, induced by a one-dimensional periodic potential, in a high-mobility GaAs two-dimensional hole system confined to a triangular quantum well. The measured oscillations exhibit two frequencies that agree well with those calculated from the Fermi contours of the two spin-split hole subbands, providing clear evidence for the observation of *spin-resolved* commensurability oscillations. [S0163-1829(99)01731-2]

Two-dimensional (2D) carrier systems whose host crystal or confinement potential lacks inversion symmetry can exhibit finite spin-splitting even in the absence of an applied magnetic field.[1–9] From early cyclotron resonance and magnetotransport data on modulation-doped GaAs/$Al_xGa_{1-x}As$ (001) quantum structures this spin-splitting is known to be much larger for 2D holes than for 2D electrons.[1,2] This fact stems from the strong spin-orbit coupling present for the 2D holes, and can be understood from subband calculations based on $\mathbf{k}\cdot\mathbf{p}$ theory.[8] 2D carrier systems with large spin-splitting have been the subject of substantial recent interest[6,7] since they are good candidates for realizing new devices such as a spin-polarized, field-effect transistor,[10] and for observing exotic physical phenomena such as Berry's phase.[11] Here we report clear evidence for spin-resolved commensurability oscillations in a 2D hole system (2DHS) confined to GaAs/$Al_xGa_{1-x}As$ interface. This system is particularly interesting since its spin-splitting can in fact be tuned via the application of a surface gate[12] thus, fullfilling another requirement for the realization of a spin-polarized, field-effect transistor.[10]

To probe the quasiballistic transport properties of the spin-split 2DHS, we measured the commensurability oscillations (CO's) induced by a one-dimensional periodic modulation potential. Consider a 2D carrier system with a circular Fermi contour subjected to a one-dimensional periodic potential of period a and perpendicular magnetic field B. If the carriers can complete their classical cyclotron orbit (of radius R_c) ballistically, then the magnetoresistance along the modulation direction has a component, ΔR_{xx}, which oscillates as the orbit diameter becomes commensurate with a[13]

$$\Delta R_{xx} \propto \cos\left(2\pi\frac{2R_c}{a}-\frac{\pi}{2}\right)=\cos\left(4\pi\frac{\hbar k_f}{ea}\cdot\frac{1}{B}-\frac{\pi}{2}\right). \quad (1)$$

These oscillations can be explained by a semiclassical model,[14] which accounts for their frequency and phase extremely well. Note in Eq. (1) that the oscillation is periodic in $1/B$ with a frequency proportional to the Fermi wave vector k_f. In our spin-split 2DHS with different Fermi contours for the two spin-subbands, therefore, we may expect to see two sets of superimposed oscillations with different frequencies.

Our samples were grown on GaAs (311)A substrates by molecular beam epitaxy. They contain a 2D hole gas confined to an $Al_{0.35}Ga_{0.65}As$/GaAs interface, separated from a Si dopant layer by a 210-Å spacer. The carriers, located 1000 Å below the surface, have a typical low-temperature mobility of 1.0×10^5 cm^2/Vs and occupy only a single, spin-split hole subband in the range of densities that we studied. To induce a periodic potential modulation, an array of PMMA strips along the $[01\bar{1}]$ direction was defined by standard electron beam lithography technique on a Hall bar structure aligned along the $[\bar{2}33]$ direction. The top part of Fig. 1 schematically shows the structure of our sample. The array has a period $a=2000$ Å, while the PMMA strips are 1000-Å thick and 1000-Å wide. We then cover the entire sample surface with 50 Å of Ti and 2000 Å of Au, which is used as the front gate. A periodic modulation is created in the 2DHS under the array of PMMA strips since the part of the gate, which rests on top of the PMMA is not as effective in changing the 2DHS density as the part that directly touches the sample surface. Longitudinal magnetoresistance (R_{xx}) along the periodic potential modulation, i.e., along the $[\bar{2}33]$ direction was measured, as a function of B, at $T\approx20$ mK via a standard low frequency lock-in technique.

Figure 1 shows typical low-B R_{xx} traces measured at different applied front gate biases. We shifted the traces by their zero-B value, $R_{xx}(B=0)$, for clarity. The traces are labeled by their total hole densities, p^t, deduced from the quantum Hall effect observed at higher magnetic field, $2<B<16$ T.[15] COs are clearly seen for $0.2<B<1$ T. The Fourier spectrum of the COs is deduced from the Fourier transformation of the measured R_{xx}, in the range $0.2<B<1$ T, after subtracting a second-order polynomial background and multiplying by a smoothing window. The Fourier power spectra of these CO's are shown in Fig. 1(b). Two well-separated frequency com-

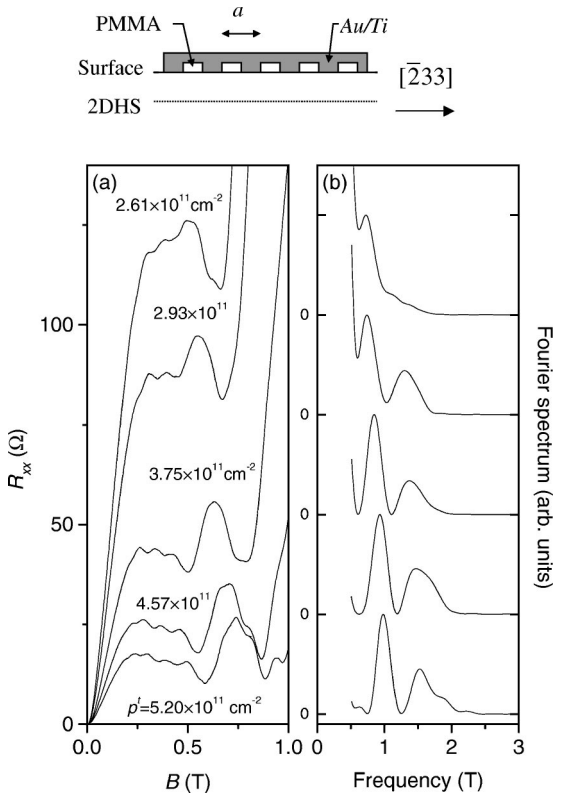

FIG. 1. (a) CO's measured along the [$\bar{2}$33] direction. The traces are marked by the total density of holes, p^t, and are shifted vertically by their respective zero-B R_{xx} value: 66 Ω for the $p^t=5.20\times10^{11}$ cm^{-2} curve, and 78, 103, 149, and 193 Ω for the lower density traces. (b) Fourier power spectra of the traces in (a). Curves are normalized to their maximum value and shifted vertically for clarity. The sample structure used in this experiment is shown on top.

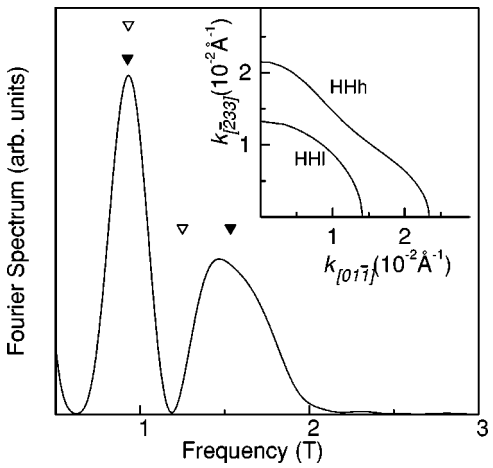

FIG. 2. Fourier power spectrum of CO's and the calculated Fermi contours of the spin-split hole subbands (inset) at $p^t=4.57\times10^{11}$ cm^{-2}. The calculated CO frequencies ($f^{l,h}_{calc}$) for these Fermi contours are marked by two solid triangles. The two hollow triangles mark $f^{l,h}_{SdH}$; these are CO frequencies based on HHh and HHl subband densities (deduced from SdH measurement) and assuming *circular* Fermi contours. The good agreement between $f^{l,h}_{calc}$ and the experimental data reveals the importance of the ''warped'' nature of the Fermi contour for the HHh band.

ponents, whose peak frequencies evolve with p^t, are observed for $p^t>2.61\times10^{11}$ cm^{-2}. We will demonstrate in the rest of this paper that the two frequency components of these CO's indeed correspond to the CO's of holes in two spin subbands.

To show this correspondence, we compare the measured frequencies with the expected CO's frequencies based on the measured spin-split subband densities. Figure 2 shows the Fourier power spectrum of CO's when $p^t=4.57\times10^{11}$ cm^{-2}. At this p^t, from an analysis of the low-B Shubnikov–de Haas (SdH) oscillations,[12] measured in a similar sample (from the same grown wafer) but without periodic modulation potential, the hole densities of the two spin-split subbands are determined to be $p^l=1.6\times10^{11}$ cm^{-2} and $p^h=2.9\times10^{11}$ cm^{-2}. According to Eq. (1), the frequencies of CO's are expected to be $f^{l,h}_{circular}\equiv2\hbar\sqrt{4\pi p^{l,h}}/ea$ if circular Fermi contours are assumed. Thus, for $a=2000$ Å, the frequencies of CO's corresponding to p^l and p^h are expected to be $f^{l}_{circular}=0.93$ and $f^{h}_{circular}=1.25$ T. The open triangles in Fig. 2 indicate these frequencies. It can be clearly observed that $f^{l}_{circular}$ matches the lower frequency component of the measured CO's very closely. The higher frequency component, however, does not match $f^{h}_{circular}$.

The discrepancy between $f^{h}_{circular}$ and the experimental observation can be understood if Fermi contour warping is taken into account. The inset to Fig. 2 shows the calculated Fermi contours of 2DHS ($p^t=4.57\times10^{11}$ cm^{-2}) confined to $Al_{0.35}Ga_{0.65}As/GaAs$ (311)A interface. We performed self-consistent subband calculations for the investigated samples using the generalized envelope-function approach.[16] The effects of bulk inversion asymmetry of the GaAs crystal are considered by employing an 8×8 $\mathbf{k}\cdot\mathbf{p}$ model with a basis consisting of the bulk states Γ_{6c}, Γ_{8v}, and Γ_{7v} which can be systematically derived from the $14\times14\mathbf{k}\cdot\mathbf{p}$ model of Ref. 16. This model accounts for the nonparabolicity and warping of the energy bands and allows to consider the (311) orientation of the sample. The inversion asymmetry of the $GaAs/Al_xGa_{1-x}As$ heterostructure (confining potential) is taken into account by considering the sample geometry, doping, and carrier concentration. It is important to note that all bulk band parameters for GaAs and $Al_xGa_{1-x}As$ (Ref. 17) as well as the band offsets[18] are known. Our calculations are thus essentially free of adjustable parameters. The calculations were done for zero-magnetic field.

The inset to Fig. 2 reveals that the contour is nearly circular for the lighter spin-subband (HHl band) but is significantly warped for the heavier spin-subband (HHh band).[19] For the latter, since the calculated Fermi wave vector in the [011$\bar{}$] direction is larger than $\sqrt{4\pi p^h}$ (the value for a circular Fermi contour), it is reasonable that the higher frequency component of CO's, which is measured for a potential modulation along [$\bar{2}$33], is centered at higher value than the expected $2\hbar\sqrt{4\pi p^h}/ea$; note that the frequency of the CO's is a measure of the Fermi wave vector in the direction perpendicular to the modulation direction.[20] Indeed, our calculated positions of the CO's frequencies, taking into account the warped Fermi contour, agree remarkably well with the experimental data (see solid triangles in Fig. 2).

The peak frequencies of the two frequency components

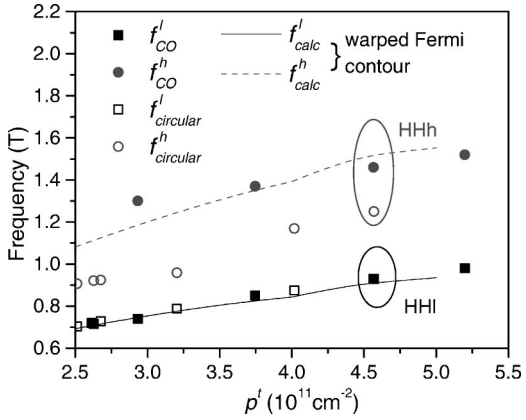

FIG. 3. Frequency vs total hole density plot for the CO's. $f^{l,h}_{CO}$: peak frequencies of Fourier power spectra shown in Fig. 1(b). $f^{l,h}_{circular}$: expected CO frequencies based on the spin-split subband densities measured by SdH oscillations and assuming circular Fermi contours. $f^{l,h}_{calc}$: expected CO frequencies deduced from the calculated Fermi contours.

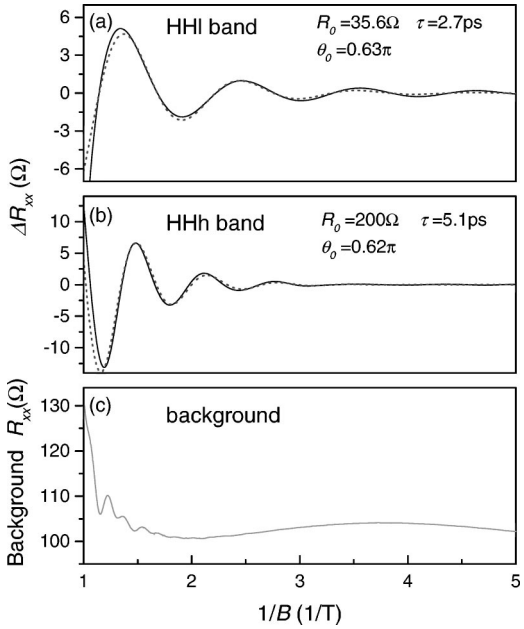

FIG. 4. Fourier decomposition of the measured CO's at $p^t = 4.57\times10^{11}$ cm^{-2}. (a) Solid curve: inverse Fourier transform of the lower frequency component shown in Fig. 2. Dotted curve: trace generated according to Eq. (2) and using fitting parameters as indicated in the figure. (b) Same analysis as in (a) is done for the higher frequency component of Fig. 2. (c) Background deduced by subtracting the original data from the sum of the solid curves in (a) and (b).

shown in Fig. 1(b), f^l_{CO} and f^h_{CO}, are summarized and plotted against p^t in Fig. 3 as solid symbols. The expected CO frequencies based on measured spin-split subband densities and assuming circular Fermi contours, $f^{l,h}_{circular}$, are shown as open symbols in the same figure. The expected CO frequencies deduced from theoretical calculation, with Fermi contour warping taken into account, are also plotted in Fig. 3 ($f^{l,h}_{calc}$). The three frequencies corresponding to *HHl* band, f^l_{CO}, $f^l_{circular}$, and f^l_{calc} agree with each other to within 4% in the entire experimental range of p^t, confirming the nearly circular shape of the *HHl* Fermi contour. For the *HHh* band, on the other hand, the experimental CO's data can be quantitatively understood only if the warping of the *HHh* Fermi contour is taken into account: while f^h_{CO} and f^h_{calc} agree with each other to within 8%, $f^h_{circular}$ are always significantly smaller than these two frequencies. The good agreement between $f^{l,h}_{calc}$ and $f^{l,h}_{CO}$ in the entire experimental range strongly suggests that the observed CO's indeed correspond to the CO's of the spin-split subbands.

We can further separate the COs corresponding to holes in *HHl* and *HHh* bands by analyzing our data via *inverse* Fourier transformation of the individual frequency components seen in the Fourier power spectra. Figure 4 demonstrates this operation for the data corresponding to $p^t = 4.57\times10^{11}$ cm^{-2} whose Fourier power spectrum is shown in Fig. 2. The region $0.63 < f < 1.19$ T of the Fourier spectrum, which corresponds to CO's of the holes in the *HHl* band, is inverse Fourier transformed and divided by the original window function. The result is shown as the solid curve in Fig. 4(a). The second region of the spectrum, $1.19 < f < 3$ T, corresponding to CO's of holes in the *HHh* band, is analyzed in a similar fashion and the resulting inverse Fourier transform is shown in Fig. 4(b). The background shown in Fig. 4(c) is derived by subtracting the original data from the sum of the solid curves shown in Figs. 4(a) and (b). The fact that the background curve is smooth except for the high frequency SdH oscillations appearing in the $1/B < 2$ T^{-1} region assures that Fourier decomposition technique does not introduce any major artifacts.

The separated *HHl* and *HHh* band CO's can be analyzed by a simple empirical expression, which assumes that the amplitude of CO's decays exponentially with $1/B$, in analogy to the SdH oscillations (the Dingle factor)[21]

$$\Delta R_{xx} = R_0 \exp(-\pi/\omega_c\tau)\cos\left(2\pi f^{l,h}_{calc}\cdot\frac{1}{B}-\theta_0\right), \quad (2)$$

where R_0, τ, and θ_0 are fitting parameters, $\omega_c = eB/m^*$ is the cyclotron frequency, and $f^{l,h}_{calc}$ are fixed parameters as defined in Fig. 3. The results of the best fits are shown as dotted curves in Figs. 4(a) and 4(b) together with the fitting parameters. Note that the fitting parameters for the phase of the oscillations, $\theta_0 = 0.63\pi$ and 0.62π for CO's of *HHl* and *HHh* holes respectively, are close to the expected value 0.5π according to Eq. (1) ($\approx 0.13\pi/2\pi = 7\%$ difference of a full cycle). This observation further confirms that we are indeed measuring and are able to separate, via Fourier analysis, CO's of both *HHl* and *HHh* holes. In addition to this confirmation, from an analysis of the exponential B dependence of the CO's amplitude [the $\exp(-\pi/\omega_c\tau)$ term in Eq. (2)],[21] we also estimate the scattering times (τ) to be 2.7 ps for holes in *HHl* band and 5.1 ps for holes in *HHh* band. In order to obtain these estimates, we used the band structure shown in the inset to Fig. 2 and the relation $m^* = \hbar^2/2\pi \cdot \partial A/\partial E$, where A is the area enclosed by Fermi contour and E is energy, to estimate the cyclotron effective mass (m^*) of *HHl* and *HHh* holes to be $0.22m_0$ and $0.65m_0$, respectively. At the moment we do not have a quantitative understanding of the magnitude of these scattering times;[22] we note however that they are comparable to scattering times deduced

from similar CO measurements in GaAs/$Al_xGa_{1-x}As$ 2D *electron* systems.[21] It is also worth mentioning that the mobility scattering time, deduced from the zero-B resistivity of a nonmodulated 2DHS, is about 32 ps if we assume that the HHl and HHh band holes have the same mobility scattering time. It is about one order of magnitude higher than the scattering times deduced from CO measurements. This observation is, again, similar to the electron case.[21]

In conclusion, we report evidence of spin-resolved CO's in 2DHS confined to an $Al_xGa_{1-x}As$/GaAs interface. The CO's induced by a periodic modulation potential show two clear frequency components corresponding to COs of holes in the HHl and HHh bands. Both our theoretical calculations and experimental observations indicate that the Fermi contour of the HHl band is nearly circular but that of the HHh band is significantly warped.

We thank M.B. Santos for sample growth, and R.J. Warburton and K. Karrai for many useful conversations. This work was supported by the Army Research Office and the National Science Foundation.

[1] H. L. Störmer, Z. Schlesinger, A. Chang, D. C. Tsui, A. C. Gossard, and W. Wiegmann, Phys. Rev. Lett. **51**, 126 (1983).

[2] J.P. Eisenstein, H. L. Störmer, V. Narayanamurti, A. C. Gossard, and W. Wiegmann, Phys. Rev. Lett. **53**, 2579 (1984).

[3] B. Jusserand, D. Richards, H. Peric, and B. Etienne, Phys. Rev. Lett. **69**, 848 (1992).

[4] P. D. Dresselhaus, C. M. A. Papavassiliou, R. G. Wheeler, and R. N. Sacks, Phys. Rev. Lett. **68**, 106 (1992).

[5] C. Gauer, M. Hartung, A. Wixforth, J. P. Kotthaus, B. Brar, and H. Kroemer, Surf. Sci. **361/362**, 472 (1996).

[6] M. Schultz, F. Heinrichs, U. Merkt, T. Colin, T. Skauli, and S. Løvold, Semicond. Sci. Technol. **11**, 1168 (1996).

[7] J. Nitta, T. Akazaki, and H. Takayanagi, Phys. Rev. Lett. **78**, 1335 (1997).

[8] U. Ekenberg and M. Altarelli, Phys. Rev. B **30**, 3569 (1984); **32**, 3712 (1985); D. A. Broido, and L. J. Sham, *ibid.* **31**, 888 (1985); T. Ando, J. Phys. Soc. Jpn. **54**, 1528 (1985).

[9] For a review of early work, see U. Rössler, F. Malcher, and G. Lommer, in High Magnetic Fields in Semiconductor Physics, edited by G. Landwehr, Springer Series in Solid-State Sciences Vol. 87 (Springer-Verlag, Berlin, 1989), p. 376.

[10] S. Datta and B. Das, Appl. Phys. Lett. **56**, 665 (1989).

[11] A. G. Aronov and Y. B. Lyanda-Geller, Phys. Rev. Lett. **70**, 343 (1993); A. F. Morpurgo, J. P. Heida, T. M. Klapwijk, B. J. van Wees, and G. Borghs, *ibid.* **80**, 1050 (1998).

[12] J. P. Lu, J. B. Yau, S. P. Shukla, M. Shayegan, L. Wissinger, U. Rössler, and R. Winkler, Phys. Rev. Lett. **81**, 1282 (1998).

[13] D. Weiss, K. von Klitzing, K. Ploog, and G. Weimann, Europhys. Lett. **8**, 179 (1989); R. W. Winkler, J. P. Kotthaus, and K. Ploog, Phys. Rev. Lett. **62**, 1177 (1989).

[14] C. W. J. Beenakker, Phys. Rev. Lett. **62**, 2020 (1989); R. R. Gerhardts, D. Weiss, and K. v. Klitzing, *ibid.* **62**, 1173 (1989).

[15] The total density is deduced from the relation: $p^t = \nu(e/h)B_\nu$, where B_ν is the magnetic field at which the νth quantum Hall effect resistivity minimum occurs.

[16] R. Winkler and U. Rössler, Phys. Rev. B **48**, 8918 (1993).

[17] U. Rössler, Solid State Commun. **49**, 943 (1984); H. Mayer and U. Rössler, Phys. Rev. B **44**, 9048 (1991).

[18] J. Menendez, A. Pinczuk, D. J. Werder, A. C. Gossard, and J. H. English, Phys. Rev. B **33**, 8863 (1986).

[19] For similar contour plots, see G. Goldoni and F. Peeters, Phys. Rev. B **51**, 17 806 (1995).

[20] This is because the semiclassical trajectory of the ballistic carriers in real space under the influence of a perpendicular magnetic has the same shape as the constant energy contour in k space but is rotated by 90° with respect to the latter. Also, see G. Goldoni and A. Fasolino, Phys. Rev. B **44**, 8369 (1991).

[21] J. P. Lu and M. Shayegan, Phys. Rev. B **58**, 1138 (1998).

[22] We emphasize that our measured τ are of the order of impurity scattering times. Spin-flip scattering times are typically expected to be much longer. However, because of the very strong spin-orbit coupling and band mixing in GaAs 2D holes, spin-flip scattering, mediated by impurity scattering, can happen in ps time scale in our sample. Indeed, according to calculations by R. Ferreira and G. Bastard [Phys. Rev. B **43**, 9687 (1991)], for the Fermi wave vector of our sample (≈ 0.02 Å^{-1}), spin-flip time can be $\lesssim 10$ ps, comparable to our measured scattering time.